

We are IntechOpen, the world's leading publisher of Open Access books Built by scientists, for scientists

6,700

Open access books available

182,000

International authors and editors

195M

Downloads

Our authors are among the

154

Countries delivered to

TOP 1%

most cited scientists

12.2%

Contributors from top 500 universities



WEB OF SCIENCE™

Selection of our books indexed in the Book Citation Index
in Web of Science™ Core Collection (BKCI)

Interested in publishing with us?
Contact book.department@intechopen.com

Numbers displayed above are based on latest data collected.
For more information visit www.intechopen.com



Chapter

TIPRA – Three-Dimensional Integrated Progression Analyser: A New World Programme Exploring the Structure-Function Correlation in Glaucoma Using a Holistic 3-Dimensional Approach

*Prasanna Venkatesh Ramesh, Anujeet Paul,
Shruthy Vaishali Ramesh, Niranjana Karthik Senthil Kumar,
Prajnya Ray, Aji Kunnath Devadas, Navaneeth Krishna,
Meena Kumari Ramesh and Ramesh Rajasekaran*

Abstract

Glaucoma is a chronic, progressive eye disease that causes irreversible damage to the optic nerve head. Visual field loss, the functional change seen in glaucoma correlates well with structural loss in the neurosensory part of the eye involving the retinal ganglion cell layer (GCL) and retinal nerve fibre layer (RNFL). Early assessment and prevention of disease progression safeguard against visual field loss. Structural loss is evaluated via progressive stereoscopic optic disc photography and optical coherence tomography (OCT), which measures the GCL and RNFL thickness. Meanwhile, defects in visual fields indicate a functional loss. Ophthalmologists most correlate both the structural and functional data to interpret a patient's likelihood of glaucomatous damage and progression. In this chapter, we have elucidated means to correlate structural loss with functional loss in glaucoma patients from a neophyte's perspective and highlighted the finer nuances of these parameters in detail. This understanding of various terminologies related to structural and functional vision loss, along with the correlative interpretation of the structural and functional tests in a glaucoma patient, form the fulcrum of this chapter.

Keywords: Glaucoma, Structure-Function Correlation, Three-Dimensional, POAG, Optical Coherence Tomography, Visual Fields, Scanning Laser Ophthalmoscope, BMO-MRW

1. Introduction

Glaucoma is the upheaval in the structural and functional integrity of the optic nerve, whose progression can be arrested with judicious control of the intraocular pressure [1]. It includes a group of disorders characterised by chronic and progressive optic neuropathies. They exhibit characteristic morphological features at the optic nerve head and retinal nerve fibre layer which are associated with progressive loss of retinal ganglion cells leading to characteristic visual field defects [2]. Glaucoma is identified to be the leading cause of irreversible blindness on a global scale. The global prevalence among those aged 40 years and above has been estimated to be about 76 million in 2020. It is expected to keep rising to over 118 million affected patients by the year 2040. The disease shows a preference pattern for males, in comparison to females. People of African ancestry and people living in urban areas were more likely to be diagnosed with the disease than their counterparts of European ancestry and people living in rural areas [3]. The most common subtype among this group is primary open-angle glaucoma (POAG) [4]. POAG is distinctly regarded as a multifactorial optic neuropathy. The typical pathology involved is the acquired atrophy of the optic nerve and loss of retinal ganglion cells in the background of open anterior chamber angles, giving rise to specific visual field disturbances [5–8]. The level of structural alteration, correlated with functional perception, is used to assess the severity of POAG among patients. Structural alterations encompass changes involving, but not limited to, neuro-retinal rim thinning and retinal nerve fibre layer loss (RNFL). Functional alteration in POAG can indicate a change in the visual function, most commonly, a visual field loss [9]. Measurements of these structural and functional components show a wide range of variation between patients and between repeated measurements on the same patient, making this a considerable challenge to assess the true extent of glaucomatous damage [9]. In day-to-day practice, in glaucoma clinics, this is overcome by using the structural domain to support the diagnosis, made using the functional domain and vice versa.

The Structural and functional integrals of glaucoma show a progressive decline as the disease progresses [10]. This decline shares a common pathophysiological pathway, which includes the death of the retinal ganglion cells and their axons, thereby alluding to the possibility of a defined relationship between these two integrals. Hence, establishing this relationship between structural and functional pathology of glaucoma, and their clinical measurements, gain weight in the practice of glaucoma management [11].

2. Importance of the structure: Function relationship in glaucoma

Delving into both the structural and functional progression of glaucoma, particularly in cases of POAG, while ascertaining the natural history of the disease to grade its severity is vital. These factors dictate and influence the course of treatment, as well as the visual prognosis of said patients.

The natural history of POAG includes progressive loss of the neuro-retinal rim width on the structural front coupled with progressive loss of the visual field on the functional front [12]. In a subset of patients, it was found that blindness was an imminent problem, whose risk depended on the severity of the disease at initial presentation [13].

However, in the grading of the severity, clinical dilemmas arise when there are discrepancies between the structural and functional presentation of the disease in the same patient. For instance, some patients who show end-stage glaucomatous optic atrophy do not show an equivalent representative severity of visual field loss. On the other end of the spectrum, patients with visual field loss characteristic of severe glaucoma do not show comparable structural defects [14, 15]. Such differences pose a diagnostic predicament to a glaucoma clinician on whether to base or judge the likelihood of the disease and severity on one component over the other, or a combination of both.

3. Evolution of fundus photography

The first historical fundus photograph dates back to 1886, published by Jackman and Webster [15]. However, the major limitation of this technique was a prominent corneal reflex, resulting in poor image clarity. By 1898, Thorner designed the first reflex-free ophthalmoscope based on a simple principle of viewing the transmitted and reflected beams through either half of a dilated pupil [16]. In the following year, Friedrich Dimmer further developed a relatively more complex ophthalmoscope in partnership with Zeiss Jena. Though a significant leap forward, this ophthalmoscope was large, hefty, and significantly more expensive [17, 18]. By 1925, the Zeiss-Nordensen retinal camera, which used a carbon arc lamp for imaging, was commercially made available. The Zeiss Littmann ophthalmoscope, invented in 1955 with an improved optical design and electronic flash illumination, ushered in a new era of fundus photography.

3.1 Scanning laser ophthalmoscope

The inception of the first scanner laser ophthalmoscope opened a third door in fundus photography. Designed by Webb, Hughes and Pomerantzeff, it required substantially less light than conventional ophthalmoscopes or fundus cameras. A laser beam of $<100 \mu\text{W}$ provided a flying spot on the subject's retina, allowing an inversion of the usual division of the pupil; only the central half-millimetre is required for illumination, while the remaining area is used for light collection. No optical image of the retina is formed, but a photomultiplier tube in a pupillary conjugate plane provides video signals to a TV monitor, displaying an image.

The natural evolution of this scanning laser ophthalmoscope has undergone many iterations since. The field of view has expanded to wide-field and ultrawide-field imaging, which encompass nearly 200° of the retina (**Figure 1**). Confocal imaging, using blue, red, red-free and infrared spectrum imaging, help visualise the retinal architecture more clearly (**Figures 2 and 3**). Autofluorescence enables the assessment of the retinal pigment epithelial (RPE) layer integrity (**Figure 3**). Non-mydratic cameras allow fundus and stereoscopic disc imaging in angle closure suspects (**Figure 4**) [19]. Red-free filtering enhances the visualisation of retinal vasculature. Blue images provide an improved view of the retinal nerve fibre layer (RNFL). The red channel allows it to penetrate the deeper layers of the choroid. Infrared light provides detailed information corresponding to the choroid.

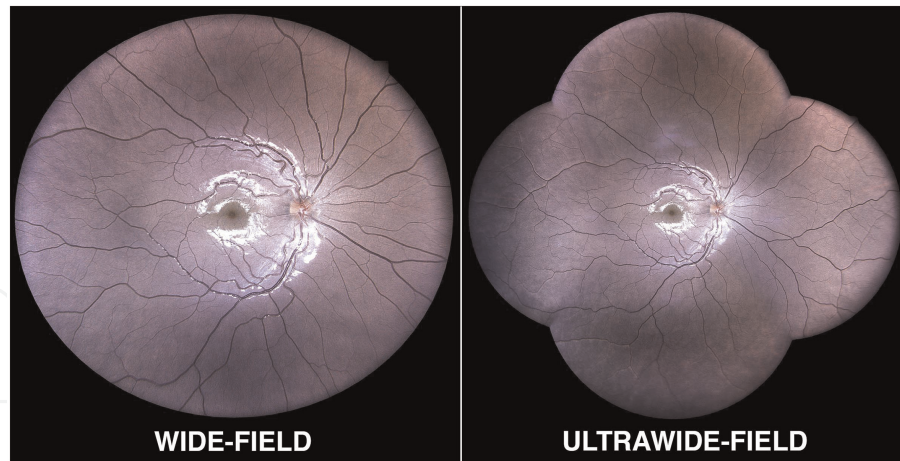


Figure 1.
Fundus photograph showing wide-field and ultrawide-field images of the same patient.

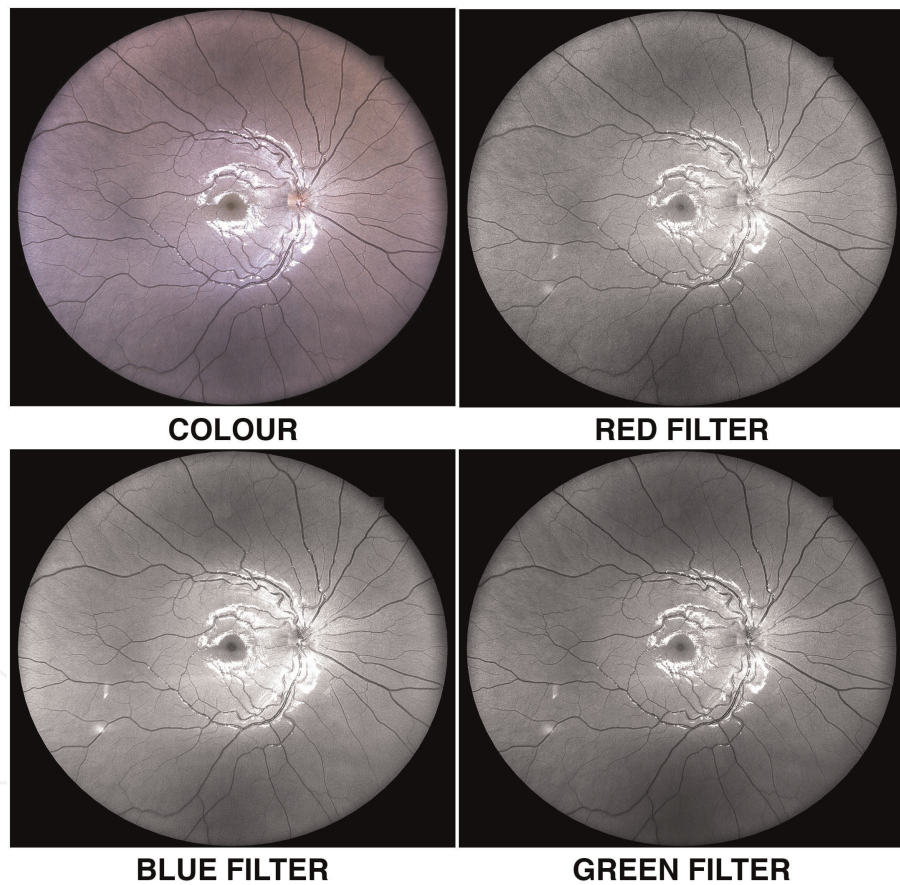


Figure 2.
Fundus photograph showing colour, red filter, blue filter & green filter images of the same patient.

4. Evolution of optical coherence tomography

Optical coherence tomography (OCT) was considered to enhance the low-coherence interferometry used initially for axial length measurements [19]. The initial systems were limited to scanning speeds of 400 axial scans (A-scans) because of a physical constraint: a moving reference mirror. Changing the position of the reference

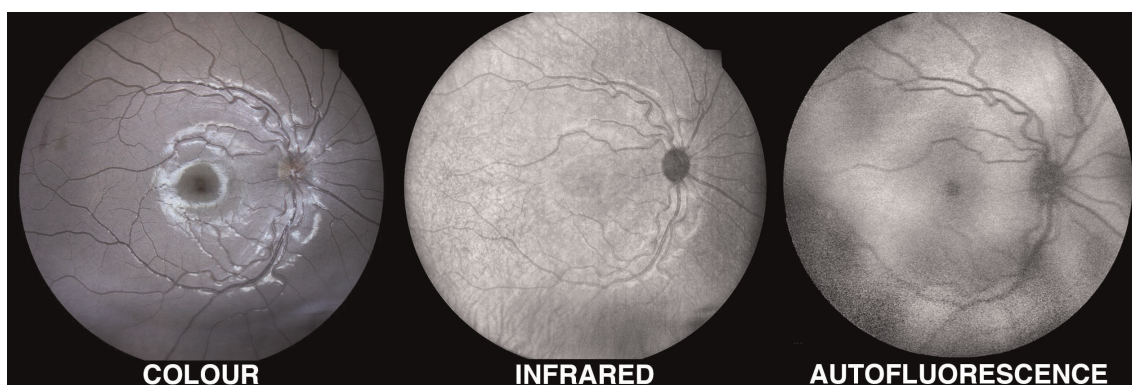


Figure 3.
Fundus photograph showing single field colour, infrared and autofluorescence image of the same patient.

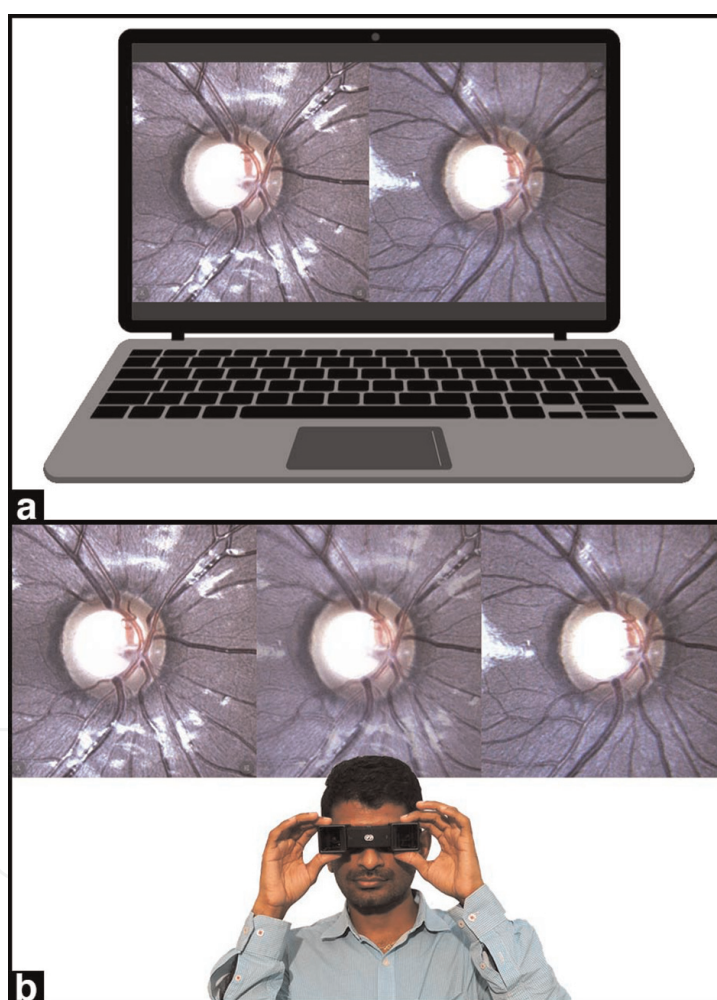


Figure 4
(a) Image showing the stereoscopic image of the right eye optic disc obtained through the fundus machine. (b) Image showing the observers' view of the stereoscopic image after wearing the 3D glasses.

mirror enabled backscattered tissue intensity levels from varying retinal and choroidal depths to be interpreted. The two main advancements incorporated into recent commercial systems are better axial resolution and increased scanning speeds [20–23]. The axial resolution was improved from 10 μ to 2 μ by incorporating broad-band light sources into the OCT systems [22]. Image acquisition speed has also been considerably improved through enhanced detection of backscattering signals without the need for

movement of the reference mirror. Frequency information is acquired with either a broad-bandwidth light source, a charge-coupled device camera, and a spectrometer or by sweeping a narrow-bandwidth source through a broad range of frequencies with a photodetector [22–28]. Spectral-domain OCT (SD-OCT) uses broadband light sources while the swept source uses a narrow bandwidth through a broad range of frequencies.

Since its inception, OCT has seen numerous advances both in image acquisition capabilities as well as image recognition abilities. Adaptive optics OCT (AO-OCT) was introduced by Miller et al. in 2003 to improve transverse resolution [29]. Adaptive optics mainly compensate for monochromatic aberrations using wavefront sensing and deformable mirrors [30]. Ultrahigh (axial)-resolution AO-OCT was introduced in 2004, improving transverse resolution to 5 to 10 μm in the retina [31]. Polarisation-sensitive OCT detects polarisation changes in polarised light to detect lesions at the level of retinal pigment epithelium layer [32]. RNFL birefringence was measured in humans by Cense et al. and Yamanari et al. who found that, unlike RNFL thickness, birefringence does not change as a function of increasing radius from the ONH [33–35]. This is likely to play a role in better OCT image acquisition, going forward. Intraoperative OCT incorporates a 1310 nm imaging system coupled to an operating microsystem [36].

5. Evolution of visual fields

During the 5th century BC, Hippocrates observed and described hemianopia. Ptolemy attributed the visual field to be circular. Ulmus first published the first illustration of visual fields in 1602. Marriott described the blind spot for the first time with its relation to the optic disc [37–39]. Thomas Young labelled the extent of the visual field as 50° superiorly, 70° inferiorly, 60° nasally, and 90° temporally [37–39]. Non-seeing areas in the visual field were reported by Boerhaave in 1708, while Beer described the shape and location of scotomas in 1817. However, quantitative visual fields were only obtained in 1856, by Von Graefe.

Jannik Bjerrum introduced campimetry with the help of a tangent screen and, along with his assistant Henning Ronne, used different target sizes to generate multiple isopters to characterise the shape and three-dimensional characteristics of the visual field sensitivity map. In this regard, the most significant contribution was the invention of the Ganzfeld bowl perimetry by Goldmann in 1945, which provided a uniform dark background superimposed with a moving optical projection system [37–39]. Tubingher perimetry was invented by Elfried Aulhorn and Heinrich Harms, which essentially was a static perimeter capable of making temporal and spatial summations throughout the visual field. The problem with bowl perimetry was the development of artefacts related to masks and increased risks of infection. In the cases of Humphrey visual field progression cannot be overlooked. In 1974, Franz Frankhauser and co-workers developed the first automated perimeter, the Octopus [40–47].

Built-in automated tools to describe and analyse progression in the Octopus perimeter, provide the greatest advantages today (**Figure 5**). These include:

Global trend analysis: consists of four indices. They are mean defect, square root loss of variance, local defect and diffuse defect.

Cluster trend analysis: mainly evaluates the ganglion cell loss along the retinal nerve fibre layer and papillomacular bundle.

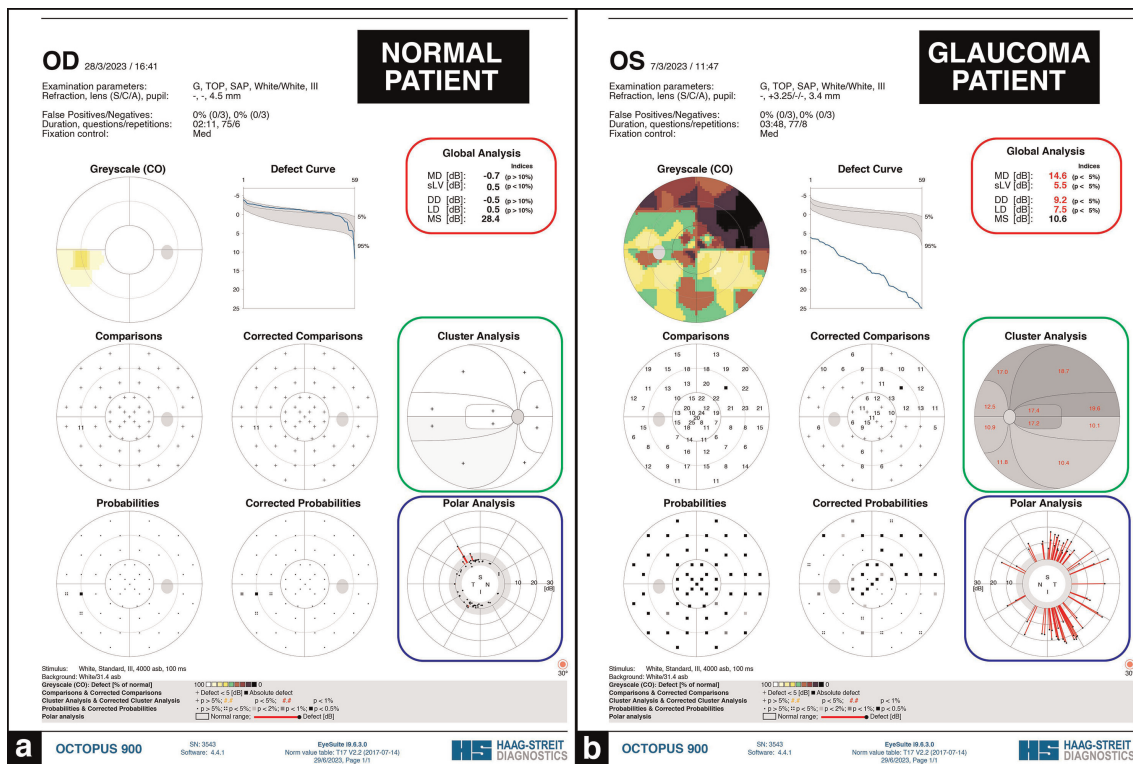


Figure 5.
 (a) Visual field report of a normal patient showing the global trend analysis (red box), cluster trend analysis (green box) and polar trend analysis (blue box). (b) Visual field report of a glaucoma patient showing the global trend analysis (red box), cluster trend analysis (green box) and polar trend analysis (blue box).

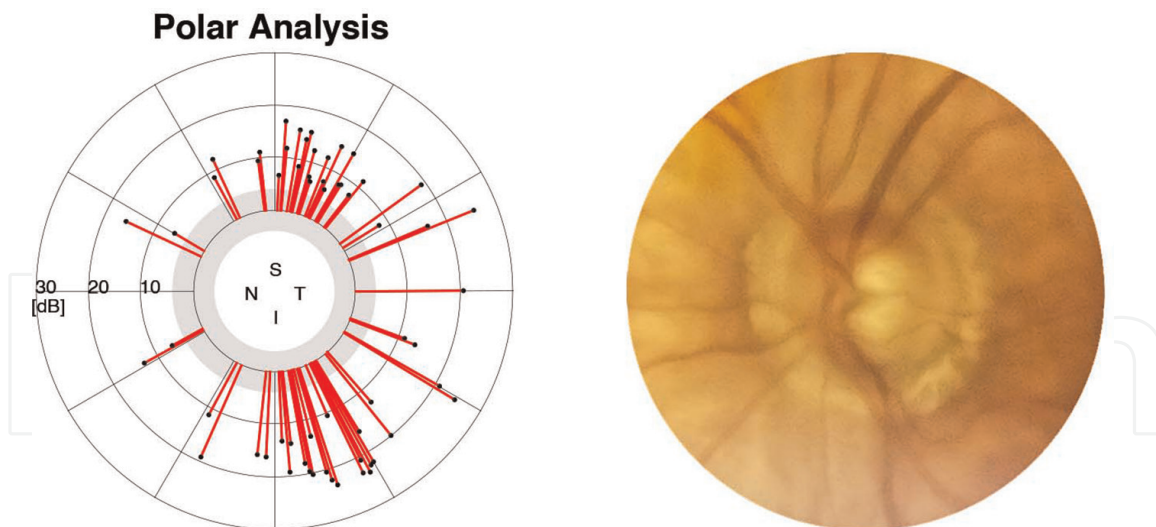


Figure 6.
 Polar trend analysis (structural) correlated with the inferotemporal notching (functional) in the optic disc.

Polar trend analysis: aids in detecting the precise location of structural defects corresponding to the functional loss that has occurred (**Figure 6**).

5.1 Short-wavelength automated perimetry (SWAP)

The colour perimeter was introduced by Hart et al., which used iso-luminant blue and yellow light, and was later termed short-wavelength automated perimetry (SWAP). It

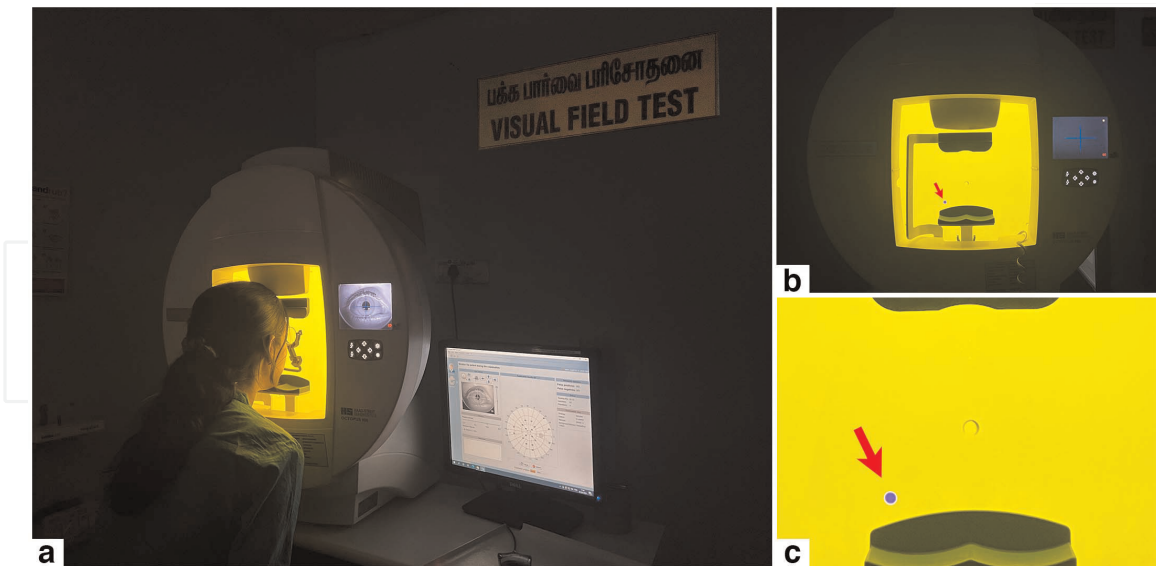


Figure 7. (a) Image showing the patient performing the SITA SWAP perimetry. (b) Image demonstrating the yellow background with blue stimulus (red arrow) and (c) zoomed view of the same with blue stimulus (red arrow).

incorporates a bright yellow background to desensitise the red and green wavelengths, thus utilizing the shorter blue wavelength as a stimulus (Figure 7) [48–52].

5.2 Flicker perimetry

Flicker perimetry is based on an intermittent flashing stimulus superimposed on a uniform background [48]. Three types of tests based on flicker perimetry aim to detect the highest rate of flicker at higher contrast, the amplitude of contrast to detect flicker, and luminance pedestal flicker. The greatest advantage of flicker perimetry is that it is unaffected by blur.

5.3 Frequency doubling threshold (FDT) perimetry

Frequency doubling perimetry incorporates a sinusoidal grating under low spatial frequency that undergoes high temporal frequency counter-flicker, thus providing double the number of light and darker bars - a frequency-doubling effect. This form of perimetry is resistant to variations occurring in the environment.

5.4 Motion perimetry

Motion perimetry is based on motion sensitivity, which is a very primitive visual function and is resistant to change in many different stimuli.

Motion perimetry is based on [48, 53].

- Determining the minimum amount of movement needed for the detection of change in position - displacement perimetry
- Evaluating the amount of motion coherence needed to detect a direction of motion from within a group of randomly moving dots - motion coherence perimetry

- Determining the direction of motion
- Assessing the velocity needed for motion detection
- Measuring the size of a number of moving dots needed to localise the direction of motion

5.5 High-pass resolution perimetry

High-pass resolution perimetry employs light and dark concentric rings, from which low spatial frequency components have been removed to emphasize the lighter and darker edges. The main aim of high-pass resolution perimetry is to elevate the detection threshold so that the detection and identification thresholds coincide simultaneously [54].

5.6 Rarebit perimetry

Very small stimuli are displayed on a video display, where 0, 1, or 2 suprathreshold stimuli are presented at different local visual field regions. The number of dots the patient was able to appreciate was then noted [55, 56].

6. The amalgamation of the three musketeers - the Spectralis, the Octopus and the EIDON

While examining the posterior pole, primarily for structural evaluation, we observe the scleral rim to determine the margin of the optic disc. However, in reality, the margins are defined by Bruch's membrane opening (BMO), which is an OCT interpretation. The Bruch's membrane opening-minimum rim width (BMO-MRW) (**Figure 8**) is a superior parameter for assessing the progression of glaucomatous damage, significantly outperforming Bruch's membrane opening horizontal rim width (BMO-HRW) [57].

Additionally, the position of the fovea may vary as a result of torsional movements of the patient's eye, potentially leading to erroneous results [58–62]. The Spectralis



Figure 8.
(a) Image showing the Bruch's membrane—minimum rim width analysis in Spectralis OCT of a normal patient. (b) Image showing the Bruch's membrane—minimum rim width (reduced) analysis in Spectralis OCT of a glaucoma patient.

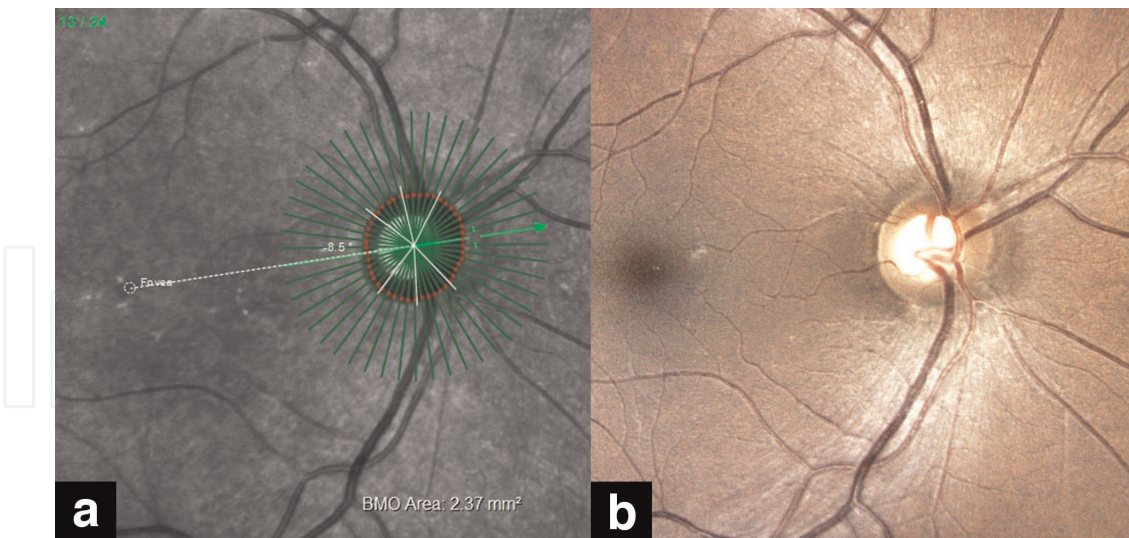


Figure 9. (a) Fovea Bruch's membrane opening axis (FoBMO) measured using the anatomical positioning system. (b) Fundus image of the same showing the fovea.

OCT incorporates an anatomical positioning system technique for precise marking of the fovea Bruch's membrane opening axis (FoBMO) (**Figure 9**). This process includes marking the centre of the fovea and BMO-MRW, formation of the FoBMO axis, and analyzing parameters related to it. This approach effectively eliminates errors resulting from torsional eye movements.

BMO MRW components:

- Black line: Measured BMO MRW
- Grey curve: Baseline values
- Horizontal axis: Position along optic disc circumference in degrees

Confocal scanning laser ophthalmoscope uses three display options:

- BMO points and section images
- BMO display points
- OCT section image

The functional correlation of the BMO-MRW is compared with the polar analysis of the OCTOPUS perimeter.

6.1 Polar trend analysis

Polar trend analysis assesses the point-wise trend analysis of the sensitivity loss in decibels, instead of a slope method to determine the rate of change. Sensitivity loss for the first visual field is represented as blue, while the last field is depicted as yellow. These two points are based on the trend lines, not the individual visual fields on that day. The two sensitivity lines are then plotted on a polar grid and are connected by a

straight line corresponding to the position of nerve fibre bundles of the test location. If there is a worsening in sensitivity between the first and last points, then it is represented as a red bar. Improvement is depicted as a green bar. The grey band in the centre indicates the normal range for these bars.

- Location of the bar indicates a corresponding structural area
- Length of the bar denotes the amount of sensitivity loss in dB
- Longer bars denote the greater magnitude of the effect
- Colour of the bar is red – loss of sensitivity
- Colour of the bar is green – a gain of sensitivity

6.2 Cluster trend analysis

In Cluster trend analysis, visual field locations corresponding to the same RNFL bundle are grouped in 10 visual field clusters and used to calculate the respective average Cluster Mean Defect.

- Highly likely normal clusters ($P > 5\%$) are marked with a “+” symbol, and are likely abnormal
- Cluster Mean defects are displayed in normal font ($P < 5\%$) or bold font ($P < 1\%$).
- The Corrected Cluster Analysis representation is similar, but eliminates diffuse visual field loss and solely considers local loss.

RNFL thickness measured clinically by fundus examination and true colour confocal fundus imaging (EIDON) is correlated with RNFL analysis of Spectralis OCT, which is then functionally correlated with cluster analysis of the Octopus perimeter (**Figure 10**). Similarly, the papillomacular bundle

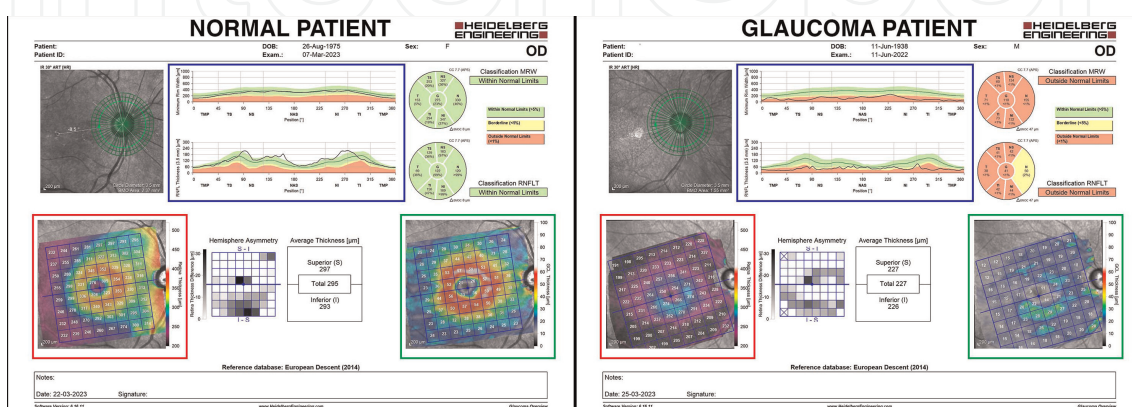


Figure 10. OCT RNFL reports of a normal and glaucoma patient respectively with RNFL thickness (red box), GCL thickness (green box), BMO-MRW and RNFL thickness comparative analysis map (blue box).

examined clinically will be correlated with the macular ganglion cell inner plexiform layer analysis of Spectralis OCT (**Figure 10**).

7. Conclusion

It is important to do a structure-function correlation to continuously monitor glaucoma progression. The structure-function correlation of optic disc analysis involves stereoscopic optic disc photography, polar analysis and BMO-MRW determination (**Figure 11**); RNFL analysis involves OCT-RNFL and 24-2 visual field analysis (**Figure 12**); GCL analysis involves OCT (GCL, Inner Plexiform Layer and facultative mRNFL), 24-2 and 10-2 visual field analysis (**Figure 13**) [63]. Each aspect of the disease can be monitored with a 3-D approach in imaging and analysis.

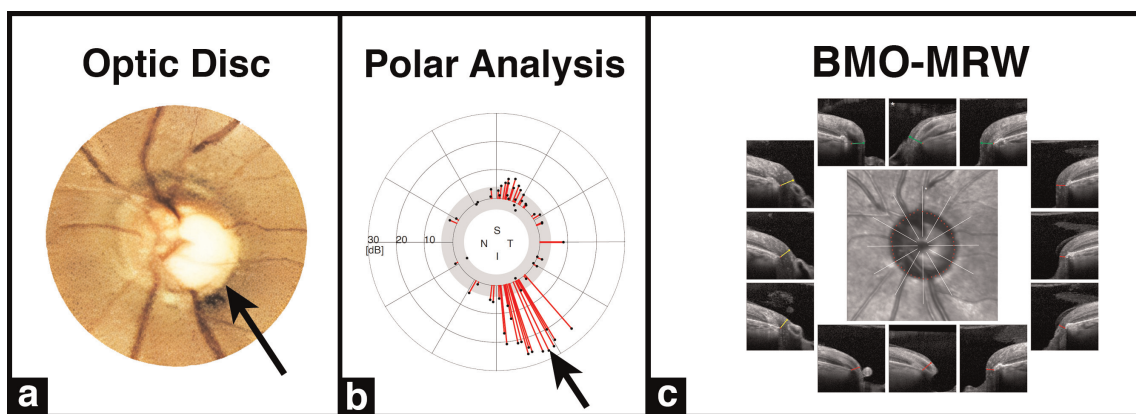


Figure 11. Image showing (a) inferior notching (black arrow) in the optic disc. (b) Corresponding inferior defect in the polar analysis map (black arrow). (c) Bruch's membrane—minimum rim width analysis in Spectralis OCT showing inferior defect.

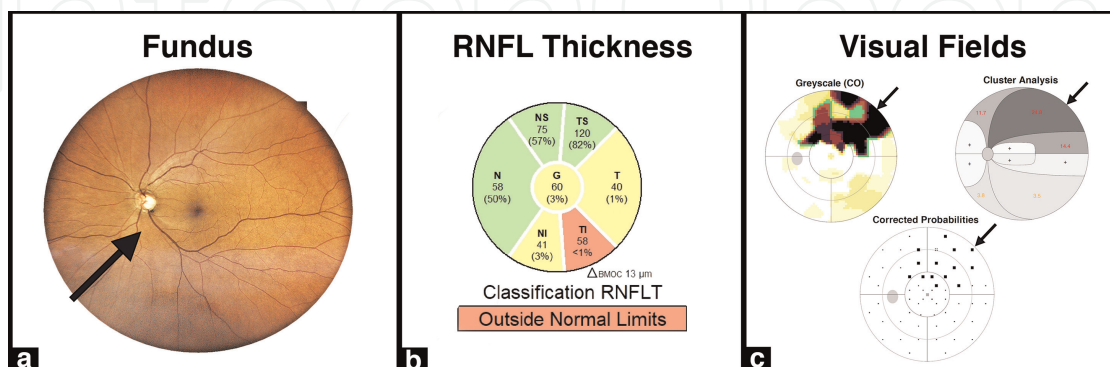


Figure 12. (a) Fundus photograph showing inferior RNFL wedge defect (black arrow). (b) RNFL thickness map showing inferotemporal thinning. (c) Visual field evaluation (greyscale, cluster analysis and corrected probabilities) showing superior visual field defect (black arrows).

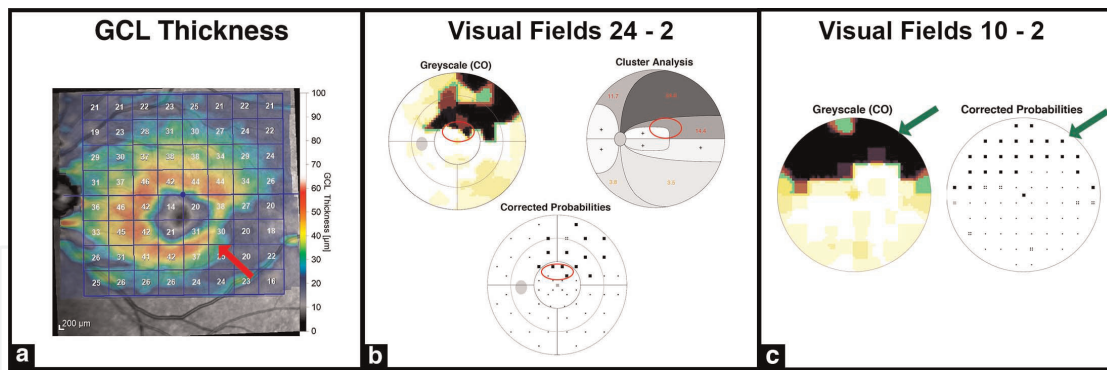


Figure 13.

(a) GCL thickness map showing inferior thinning of the ganglion cell layer (red arrow). (b) Visual field 24-2 evaluation (greyscale, cluster analysis and corrected probabilities) showing the corresponding visual field defect in the central 10 degrees of field (red circles). (c) Corresponding functional damage easily detected in visual field 10-2 (greyscale and corrected probabilities) evaluation (green arrows).

Author details

Prasanna Venkatesh Ramesh^{1*}, Anujeet Paul², Shruthy Vaishali Ramesh³,
Niranjan Karthik Senthil Kumar⁴, Prajnya Ray⁵, Aji Kunnath Devadas⁵,
Navaneeth Krishna⁵, Meena Kumari Ramesh³ and Ramesh Rajasekaran⁶

1 Department of Glaucoma and Research, Mahathma Eye Hospital Private Limited, Trichy, Tamil Nadu, India

2 Department of Vitreo-Retina, B.B. Eye Foundation, Kolkata, West Bengal, India

3 Department of Cataract and Refractive Surgery, Mahathma Eye Hospital Private Limited, Trichy, Tamil Nadu, India


4 Department of Comprehensive Ophthalmology, Nirmal Eye Hospital, Chennai, Tamil Nadu, India

5 Department of Optometry and Visual Science, Mahathma Eye Hospital Private Limited, Trichy, Tamil Nadu, India

6 Department of Paediatric Ophthalmology and Strabismus, Mahathma Eye Hospital Private Limited, Trichy, Tamil Nadu, India

*Address all correspondence to: email2prajann@gmail.com

IntechOpen

© 2023 The Author(s). Licensee IntechOpen. This chapter is distributed under the terms of the Creative Commons Attribution License (<http://creativecommons.org/licenses/by/3.0>), which permits unrestricted use, distribution, and reproduction in any medium, provided the original work is properly cited. 

References

- [1] Stamper RL, Lieberman MF, Drake MV. Chapter 1, introduction and classification of Glaucomas. In: Becker-Shaffer's Diagnosis and Therapy of the Glaucomas. 8th ed. Edinburgh: Mosby, Elsevier; 2009. pp. 1-2
- [2] European Glaucoma Society. Terminology and Guidelines for Glaucoma. 3rd ed. Savona: Editrice Dogma; 2008. Italy Editrice Dogma. p. 2008
- [3] Tham YC, Li X, Wong TY, Quigley HA, Aung T, Cheng CY. Global prevalence of glaucoma and projections of glaucoma burden through 2040: A systematic review and meta-analysis. *Ophthalmology*. 2014;**121**(11):2081-2090
- [4] Lee DA, Higginbotham EJ. Glaucoma and its treatment: A review. *American Journal of Health-System Pharmacy*. 2005;**62**(7):691-699
- [5] Prum BE, Rosenberg LF, Gedde SJ, Mansberger SL, Stein JD, Moroi SE, et al. Primary open-angle glaucoma preferred practice pattern® guidelines. *Ophthalmology*. 2016;**123**(1):P41-P111
- [6] Ramesh PV, K A, Ray P, Ramesh SV, Ramesh MK, Rajasekaran R, et al. Combating anti-glaucoma medication compliance issues among literate urban Indian population-has this fallen in our blind spot? *Journal of Clinical Ophthalmology*. 2021;**5**(S5):1-472-47
- [7] Ramesh PV, Ray P, Senthil NK, Ramesh SV, Devadas AK. Commentary: Minimally invasive glaucoma surgery for a surgical take diversion: An economic perspective. *Indian Journal of Ophthalmology*. 2023;**71**(2):566-568
- [8] Keltner JL, Johnson CA, Anderson DR, Levine RA, Fan J, Cello KE, et al. The association between glaucomatous visual fields and optic nerve head features in the ocular hypertension treatment study. *Ophthalmology*. 2006;**113**(9):1603-1612
- [9] European Glaucoma Prevention Study (EGPS) Group. Results of the European glaucoma prevention study. *Ophthalmology*. 2005;**112**(3):366-375
- [10] Read RM, Spaeth GL. The practical clinical appraisal of the optic disc in glaucoma: The natural history of cup progression and some specific disc-field correlations. *American Academy of Ophthalmology and Otolaryngology*. 1974;**78**(2):OP255-274
- [11] Ramesh PV, Ramesh SV, Ray P, Devadas AK. Commentary: The never-ending story of COVID-19: Accustoming to the new abnormal in glaucoma practice. *Indian Journal of Ophthalmology*. 2023 Mar;**71**(3):868
- [12] AGIS investigators. The advanced glaucoma intervention study (AGIS): Comparison of treatment outcomes within race: 10-year results. *Ophthalmology*. 2004;**111**(4):651-664
- [13] Grant WM, Burke JF. Why do some people go blind from glaucoma? *Ophthalmology*. 1982;**89**(9):991-998
- [14] Malik R, Swanson WH, Garway-Heath DF. "Structure-function relationship" in glaucoma: Past thinking and current concepts. *Clinical & Experimental Ophthalmology*. 2012;**40**(4):369-380
- [15] Jackman WT, Webster JD. On photographing the retina of the living eye. *Philadelphia Photographer*. 1886;**23**: 340-341 Available from: <http://www.a>

rchive.org/stream/philadelphiaph
ot18861phil#page/340/mode/1up

[16] Thorner W. A new stationary ophthalmoscope without reflexes. *American Journal of Ophthalmology*. 1899;**16**:330-345

[17] Die DF. Photographie des Augenhintergrundes. Weisbaden: Bergmann; 1907. p. 1907 Available from: <http://archive.org/details/diephotographied00dimm>

[18] Ramesh PV, Ray P, Joshua T, Devadas AK, Raj PM, Ramesh SV, et al. The photoreal new-age innovative pedagogical & counseling tool for glaucoma with 3D augmented reality (eye MG AR). *European Journal of Ophthalmology*. 2023;0(0)

[19] Ramesh PV, Parthasarathi S, Ramesh SV, Rajasekaran R, Ramesh MK. Interconnecting ophthalmic gadgets (infinity stones) at finger tips (personal computer desktop) with local area network for safe and effective practice during COVID-19 crises. *Indian Journal of Ophthalmology*. Feb 2021; **69**(2):449

[20] Drexler W, Morgner U, Kartner FX, et al. In vivo ultrahigh-resolution optical coherence tomography. *Optics Letters*. 1999;**24**:1221-1223

[21] Unterhuber A, Povazay B, Bizheva K, et al. Advances in broad bandwidth light sources for ultrahigh resolution optical coherence tomography. *Physics in Medicine and Biology*. 2004;**49**:1235-1246

[22] Wojtkowski M, Leitgeb R, Kowalczyk A, Bajraszewski T, Fercher A. In vivo human retinal imaging by Fourier-domain optical coherence tomography. *Journal of Biomedical Optics*. 2002;**7**:457-463

[23] Choma M, Sarunic M, Yang C, Izatt J. Sensitivity advantage of swept source and Fourier domain optical coherence tomography. *Optics Express*. 2003;**11**:2183-2189

[24] de Boer JF, Cense B, Park BH, Pierce MC, Tearney GJ, Bouma BE. Improved signal-to-noise ratio in spectral-domain compared with time-domain optical coherence tomography. *Optics Letters*. 2003;**28**:2067-2069

[25] Leitgeb R, Wojtkowski M, Kowalczyk A, Hitzenberger CK, Sticker M, Fercher AF. Spectral measurement of absorption by spectroscopic frequency-domain optical coherence tomography. *Optics Letters*. 2000;**25**:820-822

[26] Wojtkowski M, Srinivasan V, Fujimoto JG, et al. Three-dimensional retinal imaging with high-speed ultrahigh-resolution optical coherence tomography. *Ophthalmology*. 2005;**112**:1734-1746

[27] Choma MA, Hsu K, Izatt JA. Swept source optical coherence tomography using an all-fiber 1300-nm ring laser source. *Journal of Biomedical Optics*. 2005;**10**:44009

[28] Zhang J, Rao B, Chen Z. Swept source based Fourier domain functional optical coherence tomography. *Conference Proceedings: Annual International Conference of the IEEE Engineering in Medicine and Biology Society*. 2005;**7**:7230-7233

[29] Miller DT, Qu J, Jonnal RS, Thorn KE. Coherence gating and adaptive optics in the eye. 2003;**4956**:65-72. Available from: <https://ui.adsabs.harvard.edu/abs/2003SPIE.4956...65M>

[30] Babcock HW. The possibility of compensating astronomical seeing.

Publications of the Astronomical Society of the Pacific. 1953;**65**:229-236

[31] Hermann B, Fernandez EJ, Unterhuber A, et al. Adaptive-optics ultrahigh-resolution optical coherence tomography. *Optics Letters*. 2004;**29**: 2142-2144

[32] de Boer JF, Milner TE, van Gemert MJ, Nelson JS. Two-dimensional birefringence imaging in biological tissue by polarization-sensitive optical coherence tomography. *Optics Letters*. 1997;**22**:934-936

[33] Cense B, Chen TC, Park BH, Pierce MC, de Boer JF. In vivo birefringence and thickness measurements of the human retinal nerve fiber layer using polarization-sensitive optical coherence tomography. *Journal of Biomedical Optics*. 2004;**9**:121-125

[34] Cense B, Chen TC, Park BH, Pierce MC, de Boer JF. Thickness and birefringence of healthy retinal nerve fiber layer tissue measured with polarization-sensitive optical coherence tomography. *Investigative Ophthalmology & Visual Science*. 2004; **45**:2606-2612

[35] Yamanari M, Miura M, Makita S, Yatagai T, Yasuno Y. Phase retardation measurement of retinal nerve fiber layer by polarization-sensitive spectral-domain optical coherence tomography and scanning laser polarimetry. *Journal of Biomedical Optics*. 2008;**13**:014013

[36] Geerling G, Muller M, Winter C, et al. Intraoperative 2-dimensional optical coherence tomography as a new tool for anterior segment surgery. *Archives of Ophthalmology*. 2005;**123**: 253-257

[37] Johnson C, Wall M, Thompson H. A history of perimetry and visual field

testing. *Optometry and Vision Science: Official Publication of the American Academy of Optometry*. 2011;**88**:E8-15

[38] Lascaratos J, Marketos S. A historical outline of Greek ophthalmology from the Hellenistic period up to the establishment of the first universities. *Documenta Ophthalmologica*. 1988;**68**: 157-169

[39] Thompson HS. How visual field testing was introduced into office ophthalmology. In: David G, editor. *Cogan Ophthalmic Historical Society Meeting*. 1993

[40] Bebie H, Fankhauser F, Spahr J. Static perimetry: Strategies. *Acta Ophthalmologica*. 1976;**54**:325-338

[41] Bebie H, Fankhauser F, Spahr J. Static perimetry: Accuracy and fluctuations. *Acta Ophthalmologica*. 1976;**54**:339-348

[42] Fankhauser F, Spahr J, Bebie H. Three years of experience with the 'Octopus' automatic perimeter. *Documenta Ophthalmologica Proceedings Series*. 1977;**14**:7-15

[43] Ramesh P, Vaishali R, Ray P, Kunnath A, Ramesh M, Rajasekaran R. The curious cases of incorrect face mask positions in bowl-type perimetry versus enclosed chamber perimetry during the COVID-19 pandemic. *Indian Journal of Ophthalmology*. 2021;**69**:2236-2239

[44] Ramesh PV, Devadas AK, Senthil NK, Sainath D. Commentary: Rethinking 10-2 visual fields in early diagnosis of glaucoma for a glided glaucoma practice: The right choice to pick up a feeble noise? *Indian Journal of Ophthalmology*. 2023;**71**(3):860-863

[45] Ramesh PV, Devadas AK, Ramesh SV, Sainath D. Commentary: An

ode to the perimetrist with novel strategies for priming the patient before the psychophysical subjective perimetry test. *Indian Journal of Ophthalmology*. 2023;**71**(2):574-575

[46] Fankhauser F. Developmental milestones of automated perimetry. In: Hendkind P, editor. *ACTA: XXIV International Congress of Ophthalmology*. Philadelphia, PA: JB Lippincott; 1982. pp. 147-150

[47] Hart WM Jr, Hartz RK, Hagen RW, Clark KW. Color contrast perimetry. *Investigative Ophthalmology & Visual Science*. 1984;**25**:400-413

[48] Johnson CA, Sample PA. Perimetry and visual field testing. In: Alm A, Kaufmann P, editors. *Adler's Physiology of the Eye: Clinical Approach*. 10th ed. St. Louis, MO: Mosby; 2002. pp. 552-577

[49] Demirel S, Johnson CA. Short wavelength automated perimetry (SWAP) in ophthalmic practice. *Journal of the American Optometric Association*. 1996;**67**:451-456

[50] Johnson CA. Diagnostic value of short-wavelength automated perimetry. *Current Opinion in Ophthalmology*. 1996;**7**:54-58

[51] Sample PA. Short-wavelength automated perimetry: it's role in the clinic and for understanding ganglion cell function. *Progress in Retinal and Eye Research*. 2000;**19**:369-383

[52] Racette L, Sample PA. Short-wavelength automated perimetry. *Ophthalmology Clinics of North America*. 2003;**16**:227-236 vi-vii

[53] Wall M, Ketoff KM. Random dot motion perimetry in glaucoma patients and normal subjects. *American Journal of Ophthalmology*. 1995;**120**:587-596

[54] Keltner JL, Johnson CA. Comparative material on automated and semiautomated perimeters—1986. *Ophthalmology*. 1986;**93**:1-25

[55] Friseman L. New, sensitive window on abnormal spatial vision: Rarebit probing. *Vision Research*. 2002;**42**:1931-1939

[56] Brusini P, Salvat ML, Parisi L, Zeppieri M. Probing glaucoma visual damage by rarebit perimetry. *The British Journal of Ophthalmology*. 2005;**89**:180-184

[57] Ramesh PV, Ramesh SV, Ramesh MK, Rajasekaran R, Parthasarathi S. Striking the metronome in morphometric analysis of glaucoma - shifting from Bruch's membrane opening - horizontal rim width (BMO-HRW) to Bruch's membrane opening - minimum rim width (BMO-MRW). *Indian Journal of Ophthalmology*. 2021;**69**:1005-1008

[58] Ramesh P, Subramaniam T, Ray P, Devadas A, Vaishali R, Ansar S, et al. Utilizing human intelligence in artificial intelligence for detecting glaucomatous fundus images using human-in-the-loop machine learning. *Indian Journal of Ophthalmology*. 2022;**70**:1131-1138

[59] Ramesh PV, Ramesh SV, Aji K, Ray P, Tamilselvan S, Parthasarathi S, et al. Modeling and mitigating human annotations to design processing systems with human-in-the-loop machine learning for glaucomatous defects: The future in artificial intelligence. *Indian Journal of Ophthalmology*. 2021;**69**(10):2892-2894

[60] Ramesh PV, Ramesh SV, Devadas AK, Ramesh MK, Rajasekaran R. Response to comments on: Modeling and mitigating human annotations to design processing systems with human-in-the-loop machine learning for glaucomatous defects: The future in artificial intelligence. *Indian Journal of Ophthalmology*. 2022;**8670**(8):316461

[61] Ramesh PV, Parthasarathi S, Ramesh SV, Devadas AK, Ray P, Rajasekaran R. Decoding glaucoma module premium edition. *Indian Journal of Ophthalmology* 2022;**70**(6):2211

[62] Ramesh PV, Panneerselvan P, Devadas AK. Pick up early glaucoma: unveiling the blind truth with the 10-2 visual field. *Haryana Journal of Ophthalmology*. 2023;**XV**(1)

[63] Ramesh PV, Devadas AK, Varsha V, Mohanty B, Ray P, Balamurugan A, et al. A rare case of unilateral Axenfeld–Rieger anomaly associated with optic disc coloboma: A multimodal imaging canvas. *Indian Journal of Ophthalmology*. Jul 2022;**70**(7):2645